arXiv:quant-ph/0201051v1 13 Jan 2002

Controlling Quantum Rotation With Light

I. Sh. Averbukh*, R. Arvieu†, and M. Leibscher*
* *Department of Chemical Physics, The Weizmann Institute of Science, Rehovot 76100, Israel*
† *Institut des Sciences Nucléaires, F 38026 Grenoble Cedex, France*
e-mail: Ilya.Averbukh@weizmann.ac.il

Semiclassical catastrophes in the dynamics of a quantum rotor (molecule) driven by a strong time-varying field are considered. We show that for strong enough fields, a sharp peak in the rotor angular distribution can be achieved via time-domain focusing phenomenon, followed by the formation of angular rainbows and glory-like angular structures. Several scenarios leading to the enhanced angular squeezing are proposed that use specially designed and optimized sequences of pulses. The predicted effects can be observed in many processes, ranging from molecular alignment (orientation) by laser fields to heavy-ion collisions, and the squeezing of cold atoms in a pulsed optical lattice.

PACS numbers: 42.50.-p, 42.50.Vk, 32.80.Pj, 33.80.-b

I. INTRODUCTION

Driven rotor is a standard model in classical and quantum nonlinear dynamics studies [1]. Increasing interest in the problem has arisen because of recent atom optics realization of the quantum δ-kicked rotor [2,3], and novel experiments on molecule orientation (alignment) by strong laser fields [4–7]. A strong enough laser field creates the so-called pendular molecular states [8–10] that are hybrids of field-free rotor eigenstates. By adiabatically turning on the laser field, it is possible to trap a molecule in the ground pendular state, thus leading to molecular alignment. The only way to reach a considerable degree of alignment in this approach is by increasing the intensity of the field. However, many applications may require only a transient molecular alignment (orientation), where the molecular angular distribution becomes extremely squeezed at some predetermined moment of time. It is well known that a physically related problem of squeezed states generation in a harmonic system may be solved by a proper time-modulation of the driving force (parametric resonance excitation). Behavior of a rotor in general, strong, time-varying fields is a much less-studied problem, although it is understood that the long-persisting beats in the molecular angular distribution may be induced by short laser pulses [11–17].

In the present paper, we analyze generic features in the dynamics of a quantum rotor driven by strong pulses, and present a strategy for efficient squeezing of the rotor angular distribution by a sequence of pulses of moderate intensity. The results of our research are related to a number of physical processes, ranging from molecular alignment (orientation) by laser fields to heavy-ion collisions, and the trapping of cold atoms by a standing light wave. The paper is organized as following. Section II discusses semiclassical catastrophes in the dynamics of a driven quantum rotor with the help of a simple two-dimensional model [18]. Section III applies these generic results to a thermal system of cold atoms driven by a pulsed optical lattice [19]. Section IV focuses on 3D effects important in the processes of molecular alignment and orientation by strong laser pulses [20].

II. TWO-DIMENSIONAL ROTOR

For the sake of clarity, we start with the simplest model of a two-dimensional rotor described by the time-dependent Hamiltonian

$$\widehat{H} = \frac{\widehat{L}^2}{2I} + V(\theta, t) \tag{1}$$

where $\widehat{L}$ is the angular momentum operator, and I is the momentum of inertia of the rotor. This model contains most of the physics we want to present here. Some important additional effects that appear in 3D will be discussed below in Section IV. For a "linear 2D molecule" having a permanent dipole moment μ, and driven by a linearly polarized field, the interaction potential is

$$V(\theta, t) = -\mu\mathcal{E}(t)\cos(\theta) \tag{2}$$

where $\mathcal{E}(t)$ is the field amplitude (i. e., of a half-cycle pulse), and θ is the polar angle between the molecular axis and the field direction. In the absence of interaction with a permanent dipole moment, the external field may couple with induced anisotropic molecular polarization. This interaction (being averaged over fast optical oscillations) may result in the interaction potential proportional to $\cos^2(\theta)$ (see Eq.(17) in Section IV) [21]. Although these two forms of $V(\theta, t)$ may lead to different physical consequences (i. e., orientation vs alignment), the effects we will present are more or less insensitive to the choice of interaction. Therefore, we prefer to start with the more simple situation described by Eq.(2).

By introducing dimensionless time $\tau = t\hbar/I$, and interaction strength $\varepsilon = \mu\mathcal{E}(t)I/\hbar^2$, the Hamiltonian can be written as

$$\widehat{H} = -\frac{1}{2}\frac{\partial^2}{\partial\theta^2} - \varepsilon(\tau)\cos(\theta)$$

The wave function of the system can be expanded in the eigenfunctions of a free rotor

$$\Psi(\theta,\tau)=\frac{1}{\sqrt{2\pi}}\sum_{n=-\infty}^{+\infty}c_n(\tau)e^{in\theta}$$

In the absence of the field, the wave function takes the form

$$\Psi(\theta,\tau)=\frac{1}{\sqrt{2\pi}}\sum_{n=-\infty}^{+\infty}c_n(0)e^{-in^2\tau/2+in\theta} \tag{3}$$

Despite a simple form of Eq.(3), the wave function exhibits extremely rich space-time dynamics. In particular, it shows periodic behavior in time with the period $T_{rev}=4\pi$ (full revival) and a number of fractional revivals at $\tau=p/sT_{rev}$ (p and s are mutually prime numbers) [22]. An analytical solution valid for a general time-dependent field is unknown even for this simplest model. Much effort has been devoted to the case of extremely short field pulses ($\delta-$kicks) (see, e. g. [1], and references therein). In general, as a result of a single kick applied to the rotor at $\tau=\tau_k$, the coefficients c_n transform as

$$c_n(\tau_k+0)=\sum_{m=-\infty}^{+\infty}i^{n-m}J_{n-m}(P)c_m(\tau_k-0), \tag{4}$$

where

$$P=\int_{-\infty}^{+\infty}\varepsilon(\tau)d\tau,$$

and $J_n(P)$ is the Bessel function of the nth order. The result of multiple kicks applied at different times can be obtained by combining transformations (4) after each kick with a free evolution according to Eq.(3) between the kicks. If the kicks are applied periodically to the system with the period T_{rev}, the system does not show chaotic behavior, and the energy accumulates quadratically with time (the so-called "quantum resonance" [23,24]). It is, therefore, quite natural to examine potential accumulation of angular squeezing of the rotor wave function under the "quantum resonance" excitation. In this case, because of the exact quantum revivals at the free-evolution stages, the effect of N kicks of a magnitude P is equivalent to the action of a single strong pulse of strength NP (see, e. g. [23]). In Figure 1, we show numerically calculated time evolution of the probability density $|\Psi(\theta,\tau)|^2$ after a relatively strong kick of a magnitude $P=85$ applied at $\tau=0$. Initially the rotor was in the ground s-state ($c_n(0)=\delta_{n0}$). For the chosen values of τ, several distinct phenomena can be seen in these plots. First of all, the wave function shows an extreme narrowing in the region of small θ after some delay following the kick [Fig. 1 (b)]. The physics of this effect may be understood with the help of the following semiclassical arguments. Consider an ensemble of randomly oriented classical rotors subject to a kick. The angular velocity of a rotor located at the angle θ is

$$\omega(\theta)=-P\sin(\theta) \tag{5}$$

just after the kick, assuming negligible initial velocity. For rotors from the region of small $\theta << 1$, the acquired velocity is linearly proportional to their initial angle, so that all of them arrive at the focal point $\theta=0$ at the same time

$$\tau_f=1/P. \tag{6}$$

This phenomenon is quite similar to the focusing of light rays by a thin optical lens. For $P>>1$, the shape of the distribution at the focusing time τ_f is dictated by the aberration mechanism (deviation of the $\cos(\theta)$ potential from the parabolic one), and it is P-independent. We consider the orientation factor $O=<1-\cos(\theta)>$ (where angular brackets mean averaging over the state of rotor) as a measure of the rotor orientation. For large enough P, the time-dependent orientation factor (for the initial s-state) may be easily estimated by averaging over the initially uniform classical ensemble of rotors having the velocity distribution of Eq. (5): $O(\tau)=1-J_1(P\tau)$. Here $J_1(x)$ is Bessel function of the first order. The minimal value $O\approx 0.418$ of the orientation factor is, in fact, achieved in the post-focusing regime, at $\tau\approx 1.84\tau_f$. As seen in Fig. 1 (c), a new phenomenon can be observed in the angular probability distribution just after the focusing. Sharp singular-like features are formed in the distribution, which are moving with time. Each of these features has a typical asymmetric shape, with pronounced oscillations on one side and an abrupt drop down on the other side. Again, the origin of this effect can be traced in the time evolution of a classical ensemble of initially motionless rotors.

After a kick applied at $\tau=0$, the motion of the rotors is described by

$$\theta=\theta_0-P\sin(\theta_0)\tau \pmod{2\pi} \tag{7}$$

where θ_0 is the initial angle. For $\tau<\tau_f$ Eq.(7) represents a one-to-one mapping $\theta(\theta_0)$ [see Fig. 2 (a)]. At $\tau=\tau_f$ the curve $\theta(\theta_0)$ touches the horizontal axis [Fig. 2 (b)]. At $\tau>\tau_f$ the angle θ_0 becomes a multi-valued function of θ [Figs. 2 (c), (d)]. The classical time-dependent angular distribution function of the ensemble is given by

$$f(\theta,\tau)=\sum_a\frac{f(\theta_0^a,\tau=0)}{|d\theta/d\theta_0^a|} \tag{8}$$

The summation in Eq. (8) is performed over all possible branches of the function $\theta_0(\theta)$ defined by Eq.(7). It follows immediately from Eq.(8) that even for a smooth initial distribution, $f(\theta,\tau)$ may exhibit a singular behavior near the angles where $d\theta/d\theta_0^a \to 0$. The quantum nature of the rotor motion replaces the classical singularities by sharp maxima in the probability distribution with the Airy-like shape typical to rainbow phenomena. Indeed, this effect is similar to the formation of caustics in the wave optics [25], and rainbow-type scattering in optics and quantum mechanics [26–28]. We should stress, however, that the long-time asymptotic regimes are radically different for the classical and truly quantum motion of the rotor. Thus, contrary to the classical limit, in which the caustics exist forever, they gradually disappear in the quantum case because of the overall decay of the initial rotational wave packet. On even longer time scale, another quantum phenomenon can be seen, namely revivals and fractional revivals of the initial classical-like motion. Figs. 1 (e)-(i) show several examples of fractional foci and rainbows in the angular distribution, which is a purely quantum effect.

As we have demonstrated, a mere application of $\delta-$kicks at the condition of "quantum resonance" does not lead to accumulated angular squeezing, and the orientation is saturated at some finite asymptotic level. Here we suggest an excitation scheme that exhibits the desired accumulation property. As previously mentioned, the wave function of the rotor reaches the state of the maximal orientation (i. e., minimal O value) after a certain delay $\Delta\tau_1$ following the application of the first kick at $\tau = \tau_1 = 0$. We suggest to apply the second kick at $\tau_2 = \Delta\tau_1$. Immediately after the second kick, the system will keep the same probability density distribution. On the other hand, $\tau = \tau_2$ will no longer be a stationary point for $O(\tau) =< 1 - \cos(\theta) > (\tau)$. The orientation factor $O(\tau)$, and its derivative are continuous and periodic functions of time in the course of a free evolution. Therefore, $O(\tau)$ will reach a new minimum at some point $\tau_2 + \Delta\tau_2$ in the interval $[\tau_2, \tau_2 + T_{rev}]$. Clearly, the new minimal value of the orientation factor is smaller than the previous one. By continuing this way, we will apply short kicks at iterative time instants $\tau_{k+1} = \tau_k + \Delta\tau_k$. By construction of this pulse sequence, the squeezing effect will accumulate with time, in contrast to the "quantum resonance" excitation. This is demonstrated by Fig. 3, which shows calculated sequences $\{\Delta\tau_k\}$ and $\{< 1 - \cos(\theta) > (\tau_k)\}$ for a rotor initially in the s-state and being kicked by pulses with $P = 3$. The logarithm of the orientation factor gradually decreases, without any sign of saturation.

At the stage of a well-developed squeezing ($O << 1$), the $\cos(\theta)$ -potential may be approximated by a parabolic one. It can be easily shown (both classically and quantum mechanically) that in this limit our strategy provides the following recurrent relationships for the time intervals $\Delta\tau_k$, successive values of the angular variance $u_k =< \theta^2 >_k \approx 2O_k$ and normalized variance of the angular velocity $w_k =< (-id/d\theta)^2 >_k /P^2$:

$$\begin{aligned} \Delta\tau_k &= \frac{u_k}{u_k + w_k} \\ u_{k+1} &= u_k - \frac{u_k^2}{u_k + w_k} \\ w_{k+1} &= w_k + u_k \end{aligned} \qquad (9)$$

For large k, the last two finite-difference equations may be replaced by a system of coupled differential equations. The latter has an exact solution providing the following asymptotics: $< \theta^2 >_k \propto 1/\sqrt{k}$ and $\Delta\tau_k \propto 1/k$. This result is in good agreement with the numerically observed power-laws behavior of the graphs 3 (a) and 3 (b), and it describes correctly their slopes at $k >> 1$. We note, that in contrast to the wave optics (in which the size of the focal spot is diffraction limited), our system may be, in principle, "unlimitedly" squeezed in angle. We also note that a quasi-periodic sequence of kicks applied at $\tau_{k+1} = \tau_k + \Delta\tau_k + T_{rev}$ provides the same squeezing scenario for a quantum rotor. The introduction of the T_{rev}-shift between pulses may be useful in the practical realizations of the scenario to avoid the overlap between short excitation pulses of a finite duration.

III. SQUEEZING OF ATOMS IN A PULSED OPTICAL LATTICE

In the present Section we apply the above results to another well-known system : cold atoms interacting with a pulsed optical lattice [19]. Optical lattices are periodic potentials for neutral atoms induced by standing light waves formed by counter-propagating laser beams. When these waves are detuned from any atomic resonance, the ac Stark shift of the ground atomic state leads to a conservative periodic potential with spatial period $\lambda/2$, half the laser wavelength (for a review, see, e. g. [29]). Such lattices present a convenient model systems for solid state physics and nonlinear dynamics studies. In contrast to traditional solid state objects, the parameters of optical lattices (i. e. lattice constant, potential well depth, etc.) are easily controllable. Many fine phenomena that were long discussed in solid state physics, have been recently observed in corresponding atom optics systems. Bloch oscillations [30], or the Wannier-Stark ladder [31,32] are only few examples to mention. Time-modulation of the frequency and intensity of the constituent laser beams provide tools for effective modeling of numerous time-dependent nonlinear phenomena. Since the initial proposal [33], and first pioneering experiments on atom optics realization of the δ-kicked quantum rotor [2], cold atoms in optical lattices provide also new grounds for experiments on quantum chaos.

We describe atoms as two-level systems with transition frequency ω_0, interacting with a standing optical wave that is linearly polarized and has the frequency of ω_l. If the detuning $\Delta_l = \omega_0 - \omega_l$ is large compared to the relaxation rate of the excited atomic state, the internal structure of the atoms can be neglected and they can be regarded as point-like particles. In this approximation, the Hamiltonian for the atomic motion is

$$H(x,p,t) = \frac{p^2}{2m} - V(t)\cos(2k_l x)\,, \qquad (10)$$

where m is the atomic mass, $k_l = \omega_l/c$ is the wave number of the standing wave. The depth of the potential produced by the standing wave is $V(t) = \hbar\Omega(t)^2/8\Delta_l$, where $\Omega(t) = 2|d_z E(t)|/\hbar$ is the Rabi frequency, $\vec{d}$ is the atomic dipole moment and $E(t)$ is the time-dependent amplitude of the light field. In the case of rather short laser pulses, this Hamiltonian corresponds to that of the two-dimensional δ-kicked rotor considered in the previous Section, with $\theta = 2k_l x$. In accordance with the previous discussion, many aspects of the dynamics of this system can be explained with semiclassical arguments. Here we provide results for a classical description of atoms in a pulsed optical lattice, with thermal effects taken into account.

We performed a Monte-Carlo simulation of the dynamics of an ensemble of δ-kicked particles which were initially uniformly distributed in space and had a thermal momentum distribution. Figure 4 shows the spatial distribution of atoms at different times after a single kick. In the upper row, the initial temperature of the ensemble is zero, and we can observe focusing [Fig. 4(a)] and formation of caustics [Fig. 4(b)] as it was described in Section II. In Fig. 4(c) and (d), the average thermal energy of the initial ensemble is comparable with the energy supplied by a kick. As a result, instead of sharp peaks in the spatial distribution (like in Figure 4 (a) and (b)), we observe some broader spatial structures that are still reminiscent of the focusing phenomenon and the rainbow effect.

We examined the accumulative squeezing approach in application to the above system. The angular localization factor $O =< 1 - \cos(2k_l x) >$ introduced in Section II describes now the spatial width of atomic groups localized in the minima of the light-induced potential. In the classical limit, the localization factor after applying n kicks is given by

$$O(t_n) = 1 - \frac{1}{2\pi}\int_{-\infty}^{\infty} d\omega_0 \int_{-\pi}^{\pi} d\theta_0 \rho(\omega_0)\cos\theta_n, \qquad (11)$$

where θ_n is determined by

$$\theta_n = \theta_{n-1} + \Delta\tau_n \left(\omega_0 - \sum_{i=0}^{n-1} \sin\theta_i\right). \qquad (12)$$

Here, $\omega_0 = 2k_l v_0$, where v_0 is the initial velocity of an atom, and $\rho(\omega_0)$ describes the thermal distribution of the velocities. Figure 5 displays the amount of spatial squeezing for the series of 100 kicks for different initial temperatures. It can be seen, that after the first few kicks the localization factor demonstrates a negative power dependence as a function of the kick number (a straight line in the double logarithmic scale). Although, the system demonstrates a reduced squeezing for higher initial temperatures, the slope of all of the curves in Figure 5 is the same after the first several kicks, in full agreement with the general arguments of the previous Section (see Eqs.(9). Therefore, the accumulative squeezing scenario may be an effective and regular strategy for atomic localization even at finite temperatures.

However, this does not mean that the accumulative squeezing is the only one (or the most effective) squeezing strategy. We have studied the best localization that can be achieved with *a given number* of identical δ-kicks, by minimizing the localization factor Eq.(11) with respect to the delay times $\Delta\tau_n$ between the kicks. For clarity, we present here only the results for zero initial temperature of the atoms. Table 1 shows the best values of the localization factor found for up to five kicks, and compares them with the results of the accumulative squeezing strategy with the same number of kicks. While the maximal atomic localization that can be achieved with two pulses is almost the same for accumulative squeezing and for the optimal sequence of two pulses, the optimized results for three and more pulses are much better.

For illustration, we choose the sequence of four optimal pulses to visualize the dynamics behind the localization process. Figure 6 (a) shows the spatial distribution of the ensemble of atoms at the time of arrival of the second pulse. Note that the second pulse is not applied at the time of the maximal localization. On the contrary, the optimized procedure finds it favorable to wait after the focusing event, until the distribution becomes rather broad. The optimal four-pulse sequence we found requires applying the third and the forth pulses simultaneously, thus producing an effective "double pulse". The spatial distribution at the time of the combined third and fourth pulses can be seen in Figure 6 (b). The distribution is only slightly more localized than in Fig. 6(a), and only the last pulse (with the double strength) squeezes the ensemble at the time of the maximal localization, thus bringing most of the atoms to the optical lattice minima [see Fig. 6 (c)].

IV. ORIENTATION AND ALIGNMENT OF A 3D ROTOR

Under certain conditions, the process of molecular orientation (or alignment) by laser fields can be described by a strongly driven three-dimensional rigid rotor model. Although many features in the dynamics of 3D rotors are similar to those already discussed for the two-dimensional case, there are two principal differences that we want to emphasize. The first one may be traced in the evolution of a classical ensemble of 3D-rotors being initially at zero temperature. The probability of finding a rotor (driven by a linearly polarized field) at a certain solid angle element $\sin\theta d\theta$ is determined by the initial distribution function, $f_0(\theta_0)$ as follows:

$$f(\theta)\sin\theta d\theta = f_0(\theta_0)\sin\theta_0 d\theta_0. \tag{13}$$

Therefore, the probability density of finding a rotor at the angle θ at some latter time is

$$f(\theta) = \sum_a \frac{f_0(\theta_0^a)\sin\theta_0^a}{|d\theta/d\theta_0^a|\sin\theta}, \tag{14}$$

where the summation is done over all branches of the $\theta_0(\theta)$ function (see Section II). The probability density $f(\theta)$ has a singularity if one of the factors in the denominator is zero. As in the 2D case, the zeroes of the fraction $|d\theta/d\theta_0^a|$ give rise to the formation of the rainbow-like structures. But in addition, the geometrical factor $\sin\theta$ can get zero too, which leads to the additional singularities at $\theta = 0$ and $\theta = \pi$. This kind of singularities are responsible for the formation of the *corona* and *glory* effects in the optical and quantum-mechanical scattering [26,27].

The second difference appears at finite initial temperature of the ensemble of 3D rotors. Because of the conservation of the angular momentum projection onto the field polarization direction, an effective repulsive centrifugal force appears that prevents the rotors from reaching the exact $\theta = 0$ and $\theta = \pi$ orientations. As a result, two *holes* in the angular distribution of a driven 3D thermal ensemble should be always present at $\theta = 0$ and $\theta = \pi$ [34].

We present below the results of Monte-Carlo simulation of the dynamics of a classical ensemble of three-dimensional rotors (linear molecules) driven by a linearly polarized time-dependent field. The corresponding Hamiltonian is

$$H = \frac{1}{2mr^2}\left(p_\theta^2 + \frac{p_\phi^2}{\sin^2\theta}\right) - \mu\mathcal{E}(t)r\cos\theta, \tag{15}$$

where m is the reduced mass of the molecule, r is the (fixed) distance between the atoms, μ is permanent dipole moment, θ and ϕ are Euler angles, and p_θ and p_ϕ are related canonical momenta. For the driving field described by a $\delta-$ pulse, the equations of motion can be easily integrated (see [35]).

At zero initial temperature, $p_{\theta_0} = 0$ and $p_{\phi_0} = 0$, and the angle $\phi(t)$ is an additional constant of motion. In this case, the dynamics of the system is reduced to that of a two-dimensional rotor, beside the effect of the geometrical factor described above. Figure 7 demonstrates the time evolution of the angular distribution of an ensemble with finite initial temperature. Here, the probability of finding a rotor inside the solid angle element $\sin\theta d\theta d\phi$ is plotted on a sphere. Red color corresponds to the high probability density while the blue color presents a low probability. Initial isotropic ensemble corresponds to an uniform solid angle distribution [see Fig. 7 (a)]. In Figure 7 (b), the distribution is plotted at the "focal time" defined according to Eq.(6). In the two-dimensional case considered in the previous Sections, the distribution at the focal time is characterized by a sharp peak at $\theta = 0$ and a broad background for larger values of θ. In the three-dimensional case, the distribution has an additional sharp dip at $\theta = 0$, as discussed above. Figures 7 (c) and (d) show the angular distribution at $t > t_f$. In Fig. 7 (c) the formation of the "*corona*" around $\theta = 0$ can be seen. In addition, we can observe a ring of relatively high probability moving from the north pole to the south pole of the sphere. This ring is a three-dimensional analog of the rainbow structure modified by the thermal effects. After the ring arrives at the south pole, a singular feature appears around $\theta = \pi$, with a hole in the center caused the repulsive centrifugal force [Fig. 7 (d)]. The formation of this sharp and robust structure in the angular distribution is analogous to the glory effect in the wave optics.

All the described phenomena, namely, focusing, caustics creation, and accumulating squeezing are not specific for the simplest models considered above, but are rather common features that can be observed under general conditions of a strong excitation of the quantum rotor. Indeed, for strong enough driving field one may neglect the initial rotational energy stored in the rotor, and use the above quasiclassical ideas to describe its dynamics. The role of the initial state of the rotor (even thermally averaged) is reduced to the formation of a frozen classical-like initial angular distribution of the rotational ensemble. For example, for the dipole-type interaction, Eq. (2), the angular focusing may be analyzed by considering classical dynamics at small angles ($\theta \ll 1$):

$$\left[\frac{d^2}{d\tau^2} + \epsilon(\tau)\right]\theta = 0. \tag{16}$$

Here, $\tau = t\hbar/I$, and $\epsilon = \mu\mathcal{E}(t)I/\hbar^2$, and the initial condition is $\theta(\tau_0) = \theta_0$, $d\theta(\tau_0)/d\tau = 0$ (where τ_0 is any moment in the past before the beginning of the pulse). Focusing time τ_f is defined by $\theta(\tau_f) = 0$. Because of the linearity of Eq.(16), the position of the focusing times, and number of focusing events do not depend on θ_0, but are determined only by the properties of the pulse $\epsilon(\tau)$. This boundary problem may be solved analytically in several special cases only (for δ-pulse considered above, or for a step-like $\epsilon(\tau)$ dependence). In general, determination of focusing times requires numerical solution of Eq.(16). Based on the previous analysis, we expect that a new angular rainbow appears immediately after each focusing event.

Figure 8 shows numerically calculated time-evolution of a three-dimensional *quantum* rotor (linear molecule) coupled to the external laser field via the anisotropic polarization interaction. The time averaged value of this interaction is (see, e. g. [21,9])

$$V(\theta,t) = -1/4\mathcal{E}^2(t)[(\alpha_{\parallel} - \alpha_{\perp})\cos^2(\theta) + \alpha_{\perp}] \tag{17}$$

Here $\alpha_{\parallel}$ and $\alpha_{\perp}$ are the components of the polarizability, parallel and perpendicular to the molecular axis, and $\mathcal{E}(t)$ is the *envelope* of the laser pulse. In this case there are two opposite equilibrium directions $\theta = 0, \pi$, so the field aligns the molecules but not orients them. The applied pulse has a Gaussian shape of a finite duration (i. e. it is not a δ-kick). As seen from Fig. 8, both focusing and caustics formation occur in the system, similar to the previous consideration, with the differences attributed to another symmetry of the problem. For instance, the angular rainbows are made of moving rings located symmetrically with respect to the equatorial plane. Note, that the glory and corona are not seen because of the $\sin(\theta)$ factor incorporated into the distribution function shown in Fig. 8.

V. CONCLUSIONS

The predicted effects may be observed in a wide range of systems with strongly driven rotational degrees of freedom. Possible examples range from heavy-ion collisions (when highly excited wave packets of nuclear rotational states are produced [12]) to molecules subject to strong laser pulses, and cold atoms trapped by standing light waves. The spectacular features described in this paper may be observed in the spatial distribution of an atomic ensemble driven by pulsed optical lattices. Recently, the accumulated squeezing scenario [18] has been realized experimentally in this system [36]. Moreover, the related squeezing approaches may find application in atom lithography of ultra-high resolution [37,38]. In the case of molecules, the considered effects may reveal themselves in the angular distribution of fragments produced by intense laser-field molecular interaction. The most direct evidence can be achieved in a two-pulse experiment, in which the first strong non-resonant pulse attempts to orient (align) the molecular ensemble, while the second short delayed pulse creates fragment ions.

---

[1] F. Haake, *"Quantum Signatures of Chaos"*, Springer-Verlag, (Berlin, 1991)

[2] F. L. Moore, J. C. Robinson, C. F. Bharucha, B. Sundaram, and M. G. Raizen, Phys. Rev. Lett. **75**, 4598 (1995)

[3] H. Ammann, R, Gray, I. Shvarchuck, and N. Christensen, Phys. Rev. Lett. **80**, 4111 (1998)

[4] D. Normand, L. A. Lompre, and C. Cornaggia, J. Phys. **B** 25, L497 (1992)

[5] P. Dietrich, D. T. Strickland, M. Laberge, and P. B. Corkum, Phys. Rev. A **47**, 2305 (1993)

[6] G. R. Kumar *et al.*, Phys. Rev. A **53**, 3098 (1996)

[7] J. Karczmarek, J. Wright, P. Corkum, and M. Ivanov, *Phys. Rev. Lett.* **82**, 3420 (1999).

[8] B. A. Zon and B. G. Katsnelson, Sov. Phys. JETP 42, 595 (1976)

[9] B. Friedrich and D. Herschbach, Phys. Rev. Lett. **74**, 4623 (1995); J. Phys. Chem. **99**, 15686 (1995).

[10] W. Kim and P. M. Felker, J. Chem. Phys. **104**, 1147 (1996)

[11] C. H. Lin, J. P. Heritage, and T. K. Gustafson, Appl. Phys. Lett. **19**, 397 (1971); J. P. Heritage, T. K. Gustafson, and C. H. Lin, Phys. Rev. Lett. **34**, 1299 (1975).

[12] L. Fonda, N. Mankoč-Borśtnik, and M. Rosina, Phys. Rep. **158**, 159 (1988)

[13] P. M. Felker, J. Phys. Chem. **96**, 7844 (1992)

[14] T. Seideman, J. Chem. Phys. **103**, 7887 (1995); *ibid.* **106**, 2881 (1997)

[15] T. Seideman, Phys. Rev. Lett. **83**, 4971 (1999)

[16] J. Ortigoso *et al.*, J. Chem. Phys. **110**, 3870 (1999)

[17] L. Cai, J. Marango and B. Friedrich, Phys. Rev. Lett. **86**, 775 (2001)

[18] I. Sh. Averbukh and R. Arvieu, Phys. Rev. Lett. **87**, 163601 (2001)

[19] M. Leibscher and I. Sh. Averbukh, submitted, 2001

[20] I. Sh. Averbukh, R. Arvieu, and M. Leibscher, to be published

[21] R. W. Boyd, *Nonlinear Optics*, Academic Press, (Boston,1992)

[22] I. Sh. Averbukh and N. F. Perelman, Phys. Lett. A **139**, 449 (1989); Sov. Phys. JETP **69**, 464 (1989)

[23] F. M. Izrailev *et al.*, Proc. Conf. on Stochastic Behavior in Classical and Quantum Hamiltonian Systems, Como, Italy (Springer-Verlag, Berlin, 1977), p.334

[24] F. M. Izrailev and D. L. Shepelyansky, Dokl. Akad. Nauk SSSR **249**, 1103 (1979); Sov. Phys. Dokl. **24**, 996 (1979)

[25] Yu. A. Kravtsov and Yu. I. Orlov, *"Caustics, Catastrophes and Wave Fields"* (Springer Series on Wave Phenomena, 15), 2nd edition, (Springer-Verlag, Berlin, 1999).

[26] K. W. Ford and J. A. Wheeler, Ann. Phys. **7**, 259 (1959)

[27] M. V. Berry, Adv. Phys. **25**, 1 (1976)

[28] S. D. Bosanac, J. Chem. Phys. **95**, 5732 (1991)

[29] P. S. Jessen and I .H. Deutsch, Adv. Atm Mol. Opt. Phys. **37**, 95 (1996)

[30] M. B. Dahan, E. Peik, J. Reichl, Y. Castin, and C. Salomon, Phys. Rev. Lett. **76**, 4508 (1996)

[31] S. R. Wilkinson, C. F. Bharucha, K. W. Madison, Qian Niu, and M. G. Raizen, Phys. Rev. Lett. **76**, 4512 (1996)

[32] Qian Niu, Xian-Geng Zhao, G. A. Gerogakis, and M. G. Raizen, Phys. Rev. Lett. **76**, 4504 (1996)

[33] R. Graham, M. Schlauutmann, and P. Zoller, Phys. Rev. Lett. **45**, R19 (1992)

[34] B. A. Zon, Eur. Phys. J. **D8**, 377 (2000)

[35] H. Goldstein, *Classical Mechanics* (Addison-Wesley, Reading, 1980)

[36] M. Raizen (private communication)

[37] I. Sh. Averbukh, patent pending

[38] for a recent review of atom lithography see, e. g. a special issue on nanomanipulation of atoms, Appl. Phys. B **70**, issue 5 (2000) (D. Meschede and J. Mlynek eds)

Figure Captions:

Table 1. The table shows the minimal value of the localization factor that can be achieved with a fixed number of kicks using accumulative squeezing scenario (O_{acc}) and optimized sequence of pulses (O_{opt}).

Fig. 1. Angular distribution of a quantum rotor excited by a strong δ-kick ($P = 85$). The graphs correspond to (a) $\tau = 0.5\tau_f$, (b) $\tau = \tau_f$, (c) $\tau = 2\tau_f$, (d) $\tau = \tau_f + T_{rev}/2$, (e) $\tau = \tau_f + T_{rev}/3$, (f) $\tau = \tau_f + T_{rev}/4$, (g) $\tau = 1.8\tau_f + T_{rev}/2$, (h) $\tau = 1.8\tau_f + T_{rev}/3$, and (i) $\tau = 1.8\tau_f + T_{rev}/4$, respectively.

Fig. 2. Classical map representing the final angle θ as a function of initial angle θ_0 for (a) $\tau = 0.5\tau_f$, (b)$\tau = \tau_f$, (c) $\tau = 3\tau_f$, and (d) $\tau = 10\tau_f$.

Fig. 3. Accumulative angular squeezing. Graphs are shown in double logarithmic scale.

Fig. 4. Spatial distribution of a classical ensemble of atoms after a single δ-kick. In Figs. (a) and (b), the initial temperature, T of the ensemble is zero. In (c) and (d), $k_BT = (1/9)k_l^2[\int_{-\infty}^{\infty} V(t)dt]^2/m$, where $V(t)$ is the depth of the potential produced by the standing wave, and k_B is Boltzmann constant. Figures (a) and (c) show the spatial distribution at focal time $\tau = \tau_f$, while in figure (b) and (c) $\tau = 2.5\tau_f$.

Fig. 5. Accumulative squeezing of atoms in a pulsed optical lattice at finite temperature (classical description). The minimal localization factor as a function of the kick number is shown in double logarithmic scale. The solid line corresponds to zero initial temperature. The dashed and dotted lines correspond to $k_BT = (1/9)k_l^2[\int_{-\infty}^{\infty} V(t)dt]^2/m$ and $k_BT = (4/9)k_l^2[\int_{-\infty}^{\infty} V(t)dt]^2/m$, respectively.

Fig. 6. Spatial distribution for the optimized sequence of four δ-pulses. The upper row shows the spatial distribution averaged over 100 atomic ensembles (each containing 5000 atoms), the lower figures show the distribution of atoms in one of the ensembles. In (a), the distribution is plotted at the time of the second pulse, that is delayed by $\tau = 3.02\tau_f$ with respect to the first pulse, in (b) - at the time of the (combined) third and fourth pulses delayed by $\tau = 1.35\tau_f$ after the second pulse. Figure (c) shows the distribution of atoms at the time of the maximal squeezing.

Fig. 7. Time evolution of the angular distribution of a (classical) ensemble of δ-kicked 3D rotors at finite temperature. The probability of finding a rotor inside the solid angle element $\sin\theta d\theta d\phi$ is plotted on a sphere. Picture (a) shows the distribution at $\tau = 0$ (time of the kick). Figures (b), (c), and (d) correspond to $\tau = \tau_f$, $\tau = 3.3\tau_f$ and $\tau = 5\tau_f$, respectively. The initial temperature corresponds to $k_BT = (1/100)\mu^2 r^2[\int_{-\infty}^{\infty} \mathcal{E}(t)dt]^2/I^2$.

Fig. 8. Contour plot for the time-dependent angular distribution function $2\pi\sin(\theta)|\Psi(\theta,\tau)|^2$ of a three-dimensional rotor (molecule) subject to a strong "polarization-type" interaction, Eq.(17) with a Gaussian pulsed laser field: $\mathcal{E}^2(t)(\alpha_\parallel - \alpha_\perp)I/4\hbar^2 = 3\times 10^3\exp[-(\tau/0.01)^2]$. Here $\tau = t\hbar/I$. The molecule resides initially in the isotropic ground angular state ($J = 0, m = 0$). Angular focusing and rainbows emerging from each of the focal regions can be seen. The angular rainbows are made of moving rings located symmetrically with respect to the equatorial plane.

No of kicks	O_{acc}	O_{opt}
2	0.33	0.31
3	0.26	0.20
4	0.21	0.11
5	0.18	0.07

TABLE I.

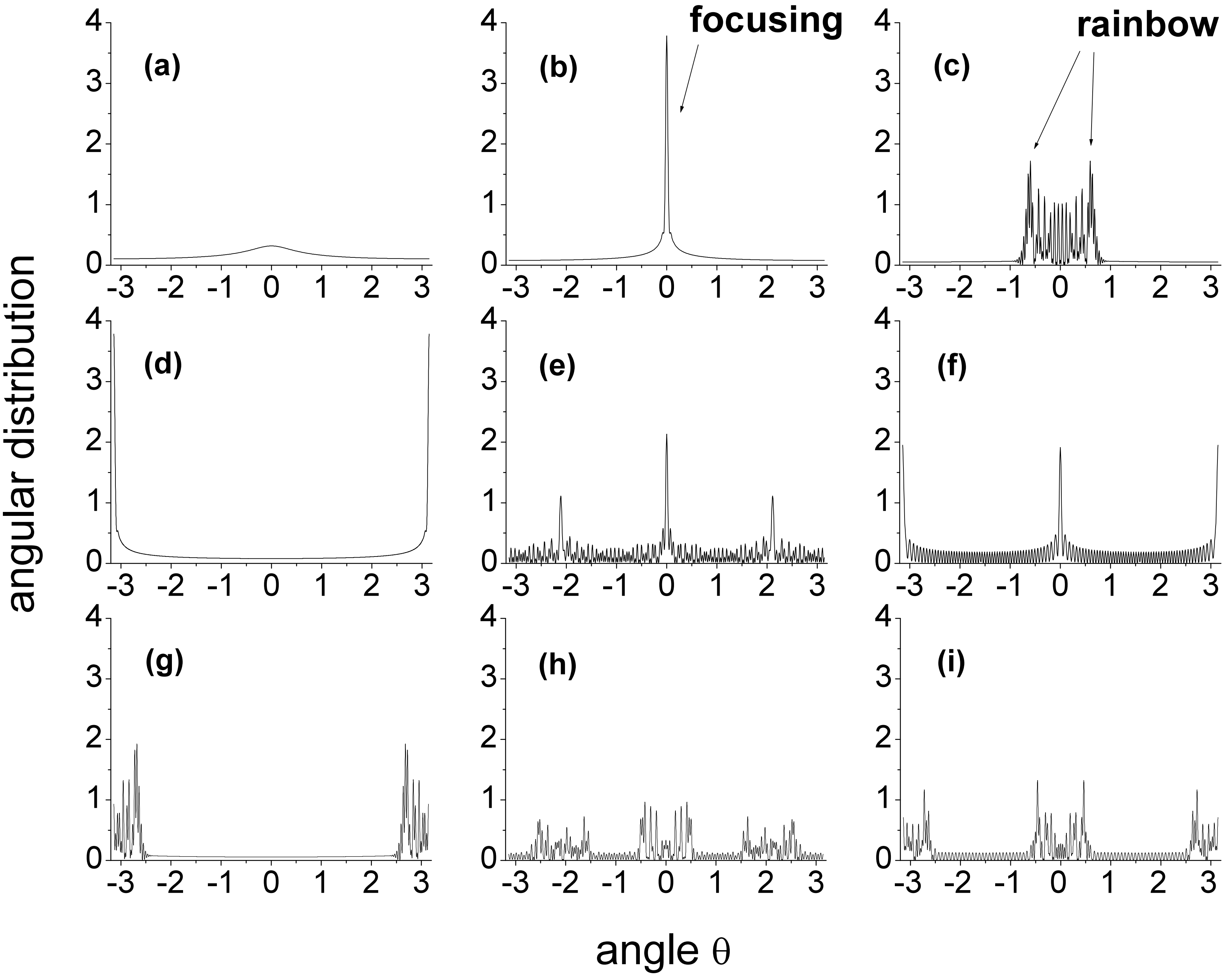

focusing
rainbow
(a)
(b)
(c)
(d)
(e)
(f)
(g)
(h)
(i)
0
1
2
3
4
-3
-2
-1
0
1
2
3
angular distribution
angle θ

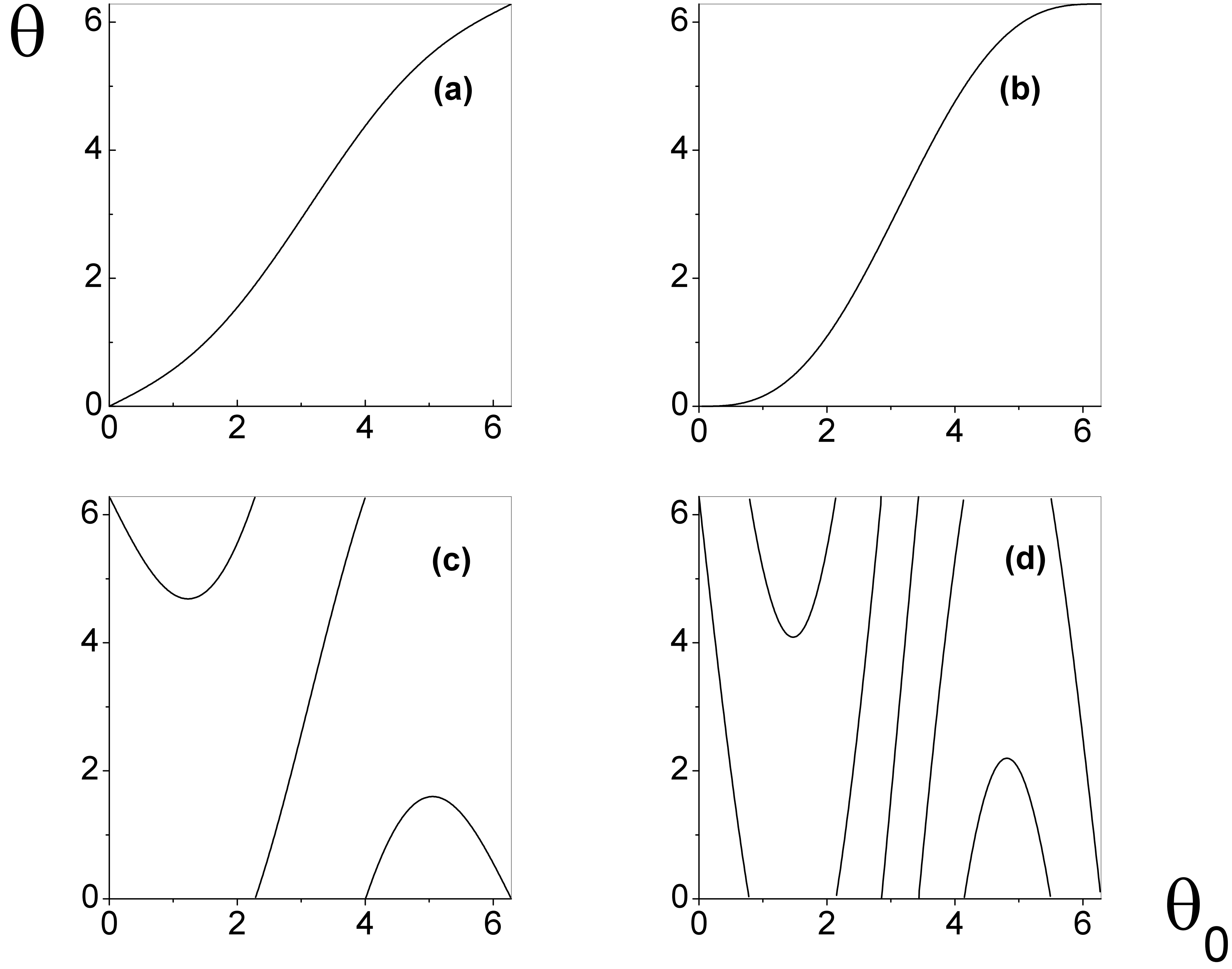
θ
(a)
(b)
(c)
(d)
0
2
4
6
0
2
4
6
θ0

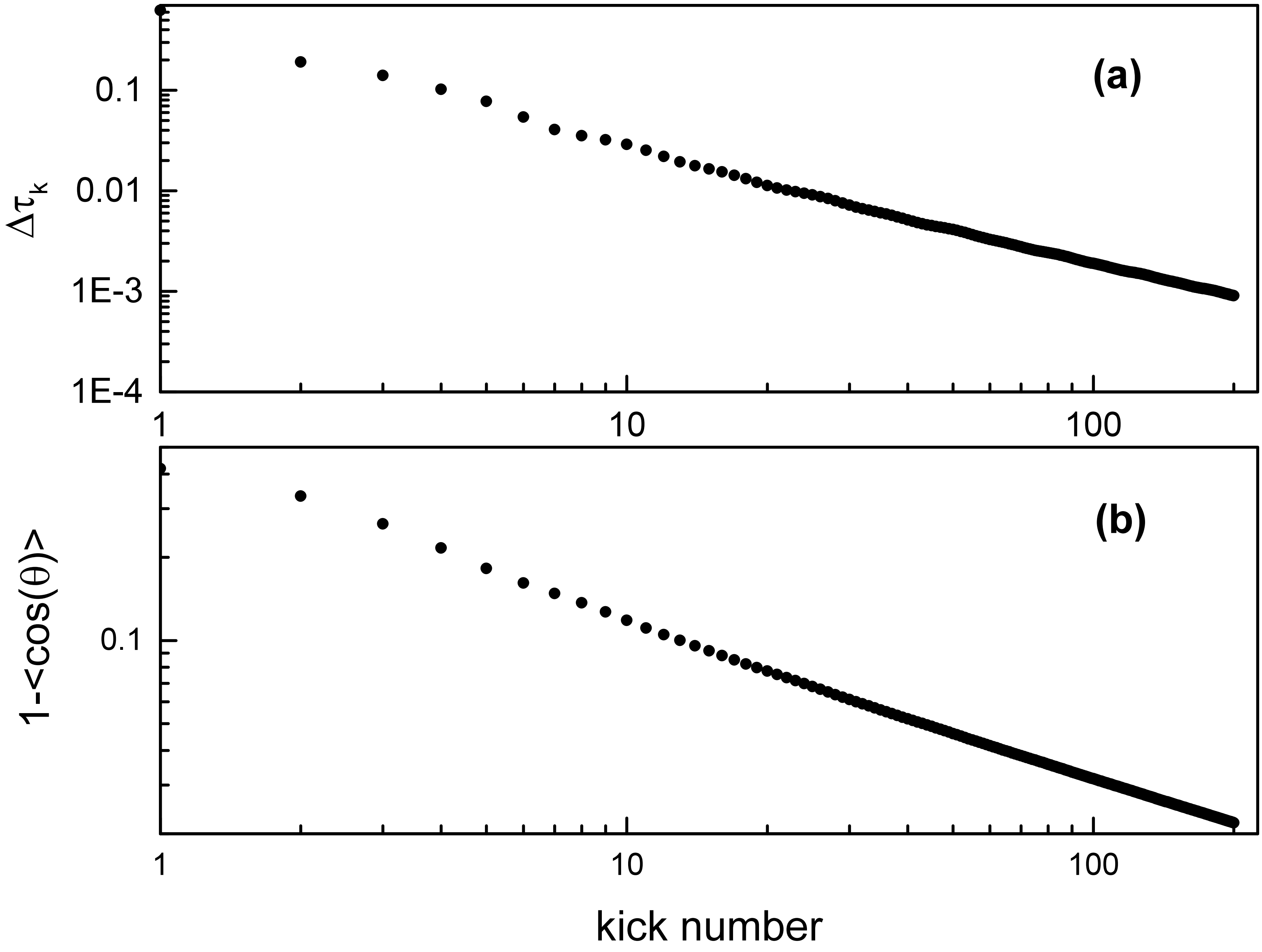
(a)
$\Delta\tau_k$
0.1
0.01
1E-3
1E-4
1
10
100
(b)
1-<cos(θ)>
0.1
1
10
100
kick number

This figure "Fig4.gif" is available in "gif" format from:

http://arXiv.org/ps/quant-ph/0201051v1

This figure "Fig5.gif" is available in "gif" format from:

http://arXiv.org/ps/quant-ph/0201051v1

This figure "Fig6.gif" is available in "gif" format from:

http://arXiv.org/ps/quant-ph/0201051v1

This figure "Fig7.gif" is available in "gif" format from:

http://arXiv.org/ps/quant-ph/0201051v1

This figure "Fig8.gif" is available in "gif" format from:

http://arXiv.org/ps/quant-ph/0201051v1